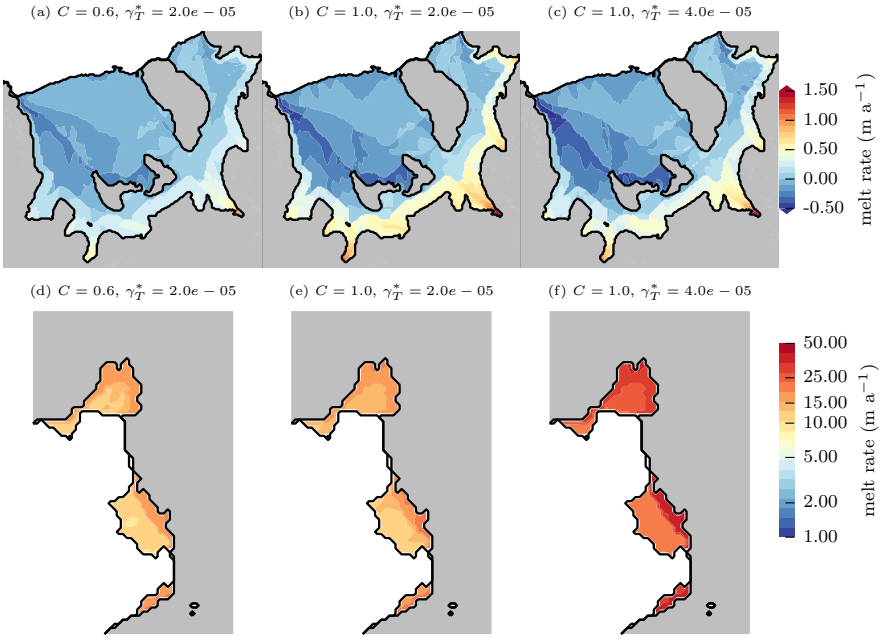

Figure S.1. Basal melt rates in the Filchner-Ronne (upper panels) and Amundsen Sea (lower panels) regions for different parameter combinations of the overturning strength C and the effective turbulent heat transfer coefficient γ_T^*. Grounded ice regions are shown in grey.

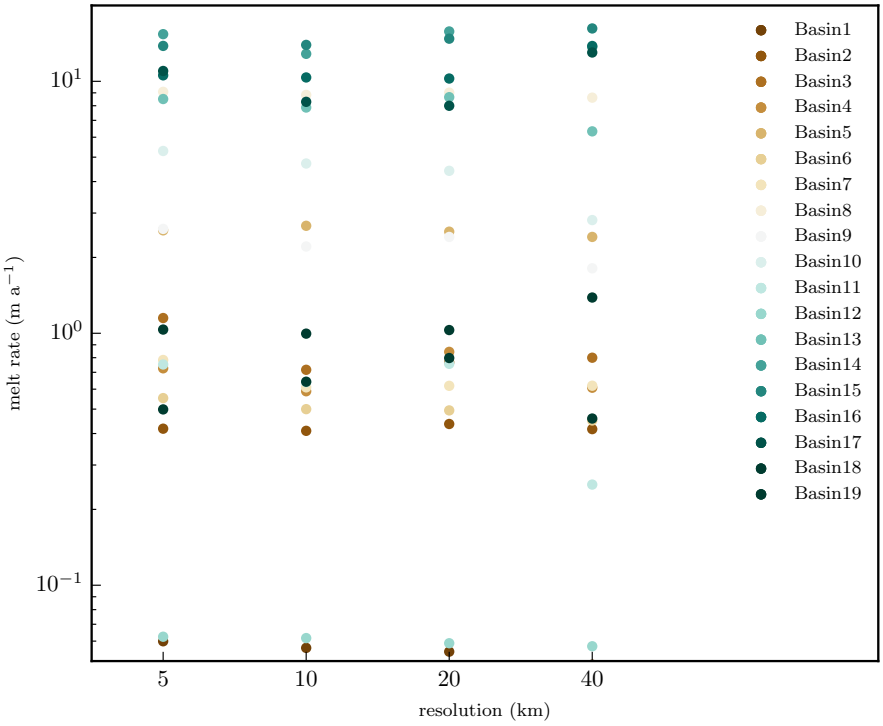

Figure S.2. Sensitivity of mean sub-shelf melt rates to the ice-sheet model resolution.

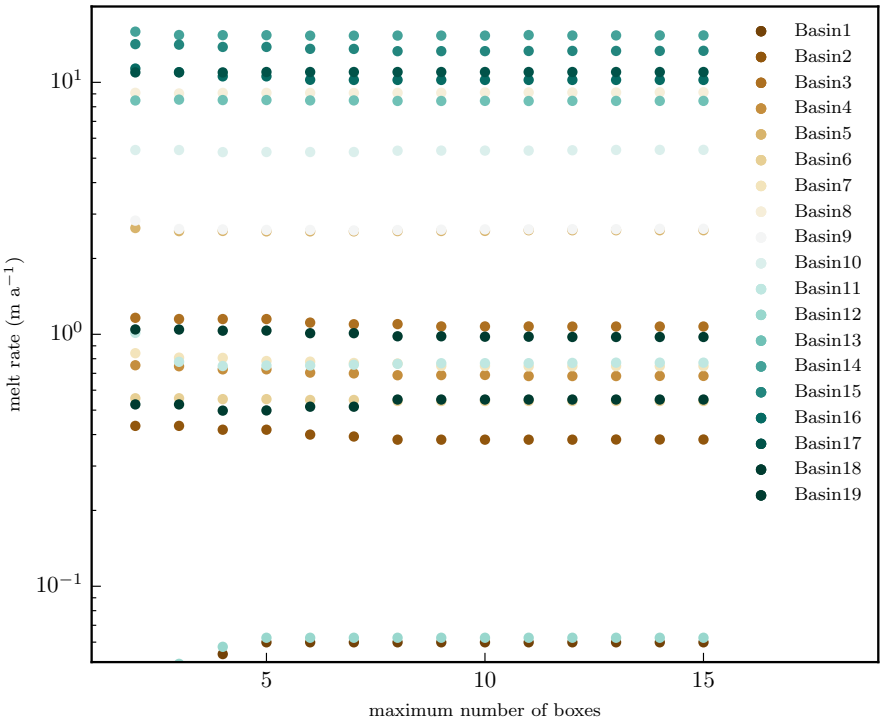

Figure S.3. Sensitivity of mean sub-shelf melt rates to the maximum number of boxes of PICO.

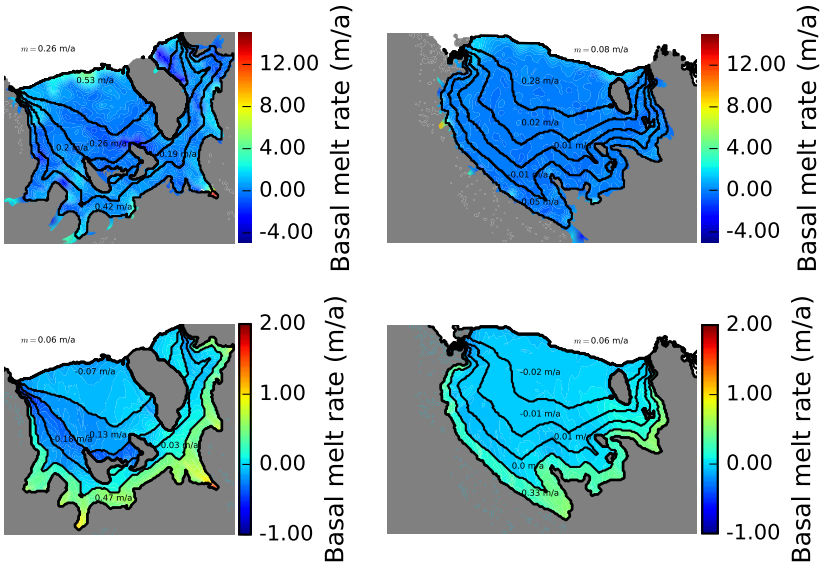

Figure S.4. Comparison of observed sub-shelf melt rates (upper row) from (Moholdt et al., 2016) with melt rates modelled by PICO (lower row) for Filchner-Ronne (left column) and Ross ice shelves (right column). Black contour lines indicate the PICO ocean boxes with annotations giving the box-wide average melt rates respectively. PICO tends to distribute melting, such that melt rate deviations are at a lower order of magnitude than in the observations. Nevertheless, box-wide averages show reasonable agreement.

Table S.1. Results from the reference simulation as displayed in Fig. 5.

basin	$m_{\sum}$	$m_{\min}$	$m_{\max}$	q	$m_{\sum}/q$	Q_{in}	Q_{out}	Q_m	Q_{Δ}	Q_{Δ}/Q_m	b_1
	$\mathrm{Gt\,a^{-1}}$	$\mathrm{m\,a^{-1}}$	$\mathrm{m\,a^{-1}}$	Sv	%	$\mathrm{TJ\,s^{-1}}$	$\mathrm{TJ\,s^{-1}}$	$\mathrm{GJ\,s^{-1}}$	$\mathrm{GJ\,s^{-1}}$	%	m
Wilkins(*)	320	0.26	19.80	0.32	3.06	361.30	357.90	3382.50	19.06	0.56	272
Pine Island	61	12.39	21.01	0.17	1.11	188.51	187.87	645.56	2.68	0.41	439
Thwaites	53	11.44	20.90	0.13	1.27	143.41	142.85	560.51	1.13	0.20	438
Getz	112	2.48	10.78	0.23	1.48	260.10	258.90	1189.23	13.98	1.18	494
Drygalski	1	0.01	3.51	0.02	0.23	17.33	17.32	12.50	-0.16	-1.28	293
Cook	7	0.70	5.25	0.05	0.38	60.87	60.80	72.20	-0.10	-0.14	458
Ninnis	4	1.08	6.61	0.04	0.31	48.80	48.75	47.19	-0.08	-0.17	514
Mertz	6	0.38	4.60	0.04	0.45	43.27	43.21	60.18	-0.14	-0.23	309
Totten	29	5.93	14.33	0.13	0.70	144.10	143.79	309.81	1.06	0.34	677
Shackleton	9	-0.21	2.70	0.07	0.40	77.62	77.52	96.93	0.48	0.50	270
West	9	-0.08	5.26	0.07	0.38	78.82	78.73	93.34	-0.17	-0.18	428
Amery	25	-1.22	5.93	0.16	0.49	175.86	175.58	269.19	11.89	4.42	674
Baudouin	22	-0.25	2.73	0.12	0.59	128.92	128.68	234.16	7.03	3.00	325
Fimbul	19	-0.25	2.97	0.10	0.57	115.85	115.64	204.02	5.79	2.84	303
Riiser-Larsen	13	-0.22	1.83	0.09	0.46	94.92	94.78	136.36	3.84	2.82	273
Brunt(**)	11	-0.16	2.30	0.08	0.40	93.81	93.69	117.21	3.31	2.83	250
Filchner-Ronne	21	-0.67	1.76	0.21	0.31	236.72	236.34	225.52	152.22	67.50	839
Ross	25	-0.24	0.62	0.17	0.44	191.38	191.01	262.62	113.98	43.40	411
Antarctica	1718	-1.22	26.91	8.51	0.62	9473.42	9454.84	18183.19	403.63	2.22	-

For each ice shelf, $m_{\sum}$ is the aggregated melt rate over the entire ice shelf, $m_{\min}$ the minimum and $m_{\max}$ the maximum melt rate within that shelf, q the overturning flux computed as average over box B_1, $m_{\sum}/q$ estimates the error in mass flux introduced by assuming constant overturning; $Q_{in} = T_0 \times q \times c_p \times \rho_w$ is the heat flux from box B_0 in box B_1, $Q_{out} = T_n \times q \times c_p \times \rho_w$ the flux from the last box B_n adjacent to the shelf front into the ocean, $Q_m = Lm_{\sum}$ the heat flux due to melting of ice, $Q_{\Delta} = Q_{in} - Q_{out} - Q_m$ the error in the heat balance. Q_{Δ}/Q_m is the error in the heat balance relative to the heat flux for melting which results from the non-linearity of the temperature solution in box B_1. The average depth of this box is given by b_1. (*) includes also Stange, Bach and George VI ice shelves and (**) also Stancomb Ice Shelf.

Video. S.1. Based on an Antarctic equilibrium state at $8\mathrm{km}$ resolution comparable to the state submitted to initMIP (Nowicki et al., 2016), PISM+PICO is forced with time-dependent ocean temperature input: Starting from equilibrium conditions, ocean temperatures increase linearly over 50 years until an ocean-wide warming of $1^{\circ}C$ is reached. It is then held constant over the next 250 model years. The movie shows the temporal evolution of the ocean temperature input for the ice shelf adjacent to Pine Island Glacier as well as the Filchner-Ronne Ice Shelf (upper left panel). The ocean temperature increase enhances the average sub-shelf melting for both ice shelves (lower left panel, shown in logarithmic scale) with the spatial distribution of the melt rates for both ice shelves on the right hand side. During the simulation, the melt rates in both areas increase, especially in the first box (upper right panel shows Filchner-Ronne Ice Shelf and lower right panel the Amundsen region). Ice-shelf thinning reduces buttressing and causes the grounding lines to retreat (for example near Foundation Ice Stream in Filchner-Ronne Ice Shelf) with the ocean boxes adjusting accordingly.